Applied Mathematics and Computation 436 (2023) 127501

Contents lists available at ScienceDirect

Applied Mathematics and Computation

journal homepage: www.elsevier.com/locate/amc

Convergence of a diffuse interface Poisson-Boltzmann (PB) model to the sharp interface PB model: A unified regularization formulation

Yuanzhen Shao[a], Mark McGowan[a], Siwen Wang[a], Emil Alexov[b], Shan Zhao[a,*]

[a] Department of Mathematics, University of Alabama, Tuscaloosa, AL 35487, USA
[b] Department of Physics and Astronomy, Clemson University, Clemson, SC 29634, USA

ARTICLE INFO

Article history:
Received 13 April 2021
Revised 27 July 2022
Accepted 20 August 2022

2010 MSC:
35J61
35Q92
35A21
35A35
Poisson-Boltzmann equation
Singular charge source
Regularization
Diffuse interface
Sharp interface convergence
Energy convergence

ABSTRACT

Both the sharp interface and diffuse interface Poisson-Boltzmann (PB) models have been developed in the literature for studying electrostatic interaction between a solute molecule and its surrounding solvent environment. In the mathematical analysis and numerical computation for these PB models, a significant challenge is due to singular charge sources in terms of Dirac delta distributions. Recently, based on various regularization schemes for the sharp interface PB equation, the first regularization method for the diffuse interface PB model has been developed in [S. Wang, E. Alexov, and S. Zhao, *Mathematical Biosciences and Engineering*, **18**, 1370–1405, (2021)] for analytically treating the singular charges. This work concerns with the convergence of a diffuse interface PB model to the sharp interface PB model, as the diffused Gaussian-convolution surface (GCS) approaches to the sharp solvent accessible surface (SAS). Due to the limitation in numerical algorithm and mesh resolution, such a convergence is impossible to be verified numerically. Through analyzing the weak solution for the regularized PB equations, the convergences for both the reaction-field potential and electrostatic free energy are rigorously proved in this work. Moreover, this study provides a unified regularization for both sharp interface and diffuse interface PB models, and clarifies the connection between this unified formulation and the existing regularizations. This lays a theoretical foundation to develop regularization for more complicated PB models.

1. Introduction

As an implicit solvent approach, the Poisson-Boltzmann (PB) model [1–3] is a widely used for studying electrostatic interactions between a macromolecule, such as protein, DNA, and RNA, and its surrounding solvent environment. Such an electrostatic analysis is indispensable for understanding various solvated biological processes at the atomic level; this includes DNA recognition, transcription, translation, protein folding, protein ligand binding, etc. By assigning partial charges at atom centers of the macromolecule, the PB model treats the solute and solvent as dielectric continuum, and assumes that the mobile ions in the water follow the Boltzmann distribution. Such a mean field approach leads to the PB equation, which is a nonlinear elliptic partial differential equation (PDE) with singular source terms [4].

* Corresponding author.
E-mail address: szhao@ua.edu (S. Zhao).

https://doi.org/10.1016/j.amc.2022.127501
0096-3003/

In the classical PB model [1–3], a two-dielectric setting is commonly assumed, i.e., the biomolecule is assigned with a low dielectric constant while the water phase is considered as a high dielectric constant medium. The solute and solvent subdomains are separated by a sharp interface, which is usually modeled as a molecular surface. Commonly used molecular surfaces include Van der Waals (VdW) surface, solvent accessible surface (SAS) [5], solvent excluded surface (SES) [6], and Gaussian surface [7]. In the sharp interface PB model, the potential and its flux are continuous across the dielectric boundary, while the normal derivative of the potential is discontinuous. Thus, special attention is needed in numerical solution of the elliptic interface problem governed by the PB equation [8,9].

Recently, several smooth solute-solvent boundary or diffuse interface PB models have been developed based on different physical and mathematical modeling approaches [10–17]. In these models, the dielectric function remains to be constants in the molecule and water regions, and changes smoothly from one constant to another over a narrow transition band or diffuse interface. It is well known that the dielectric coefficient of a medium is determined by the polarizability of the medium in responding to local electrostatic field. At the molecular level, the existence of a sharp dielectric boundary seems to be unphysical. Instead, it makes more physical sense by assuming polarizability to be a smooth function at the solute-solvent boundary. This is the physical reasoning behind the development of diffuse interface PB models [10–17]. Furthermore, heterogeneous dielectric distributions have been constructed in the PB modeling to mimic the effect of the conformational changes of the macromolecule so that the ensemble average solvation energy could be captured by using a single structure [18–21].

More recently, a Gaussian convolution surface (GCS) has been proposed in [22] to efficiently generate a diffuse interface for the PB modeling. Based on a Heaviside function defined over the SAS, a convolution with a Gaussian kernel is conducted to provide a level set function to characterize the solute and solvent subdomains, as well as the transition layer. Moreover, this convolution is realized via the fast Fourier transform (FFT), so that the complexity scales linearly with respect to the spatial degree of freedom. Thus, the GCS algorithm is very efficient in treating large protein systems. We note that the width of the Gaussian kernel or the transition layer can be controlled by the variance parameter σ. As σ goes to zero, the GCS diffuse interface will converge to a sharp interface.

In the mathematical analysis and numerical computation for both sharp interface and diffuse interface PB models, a significant challenge is due to singular charge sources in terms of Dirac delta distributions [1–3]. Mathematical analysis becomes more compliciated, because the electrostatic potential blows up at the atom centers [4,23,24]. The discretization of singular charge sources in grid based computations has drawn much attention in the PB literature. For finite difference methods, a trilinear approach is commonly used, in which the singular charges are distributed to the neighboring grid nodes with finite values [25]. In a finite element variational form, the definition of the delta function can be applied so that a point charge can be evaluated through the trial function [26]. These numerical approaches may produce an acceptable estimate of electrostatic free energy when certain error cancellation can be taken advantage of in solving both the PB equation and Poisson equation with the same singular sources [22,26]. Nevertheless, the direct discretization of the PB equation remains to be problematic from the numerical point of view, because one essentially approximates an unbounded potential solution by finite numerical values.

The regularization approach is known to be the most successful method for treating the singular charge sources of the PB equation. For the sharp interface PB model, various regularization methods have been developed [8,23,24,27–33]. The main idea of the regularization methods is to decompose the potential into two or three components, and analytically capture the singularity by using one component. This singular component is actually the Coulomb potential and satisfies a Poisson's equation with the same singular sources. Mathematically, the singular component can be expressed as Green's functions, which are unbounded at atom centers, but can be analytically calculated at other places. After removing the singular component, other potential components in all regularization methods become bounded so that their mathematical analysis and numerical computation become easier. While all regularization formulations are consistent with the original PB equation, some regularization methods are known to be significantly less accurate than the others [31]. To understand this discrepancy, four popular regularizations were analyzed and compared in [34]. Through tracking the source of error, an accuracy recovery technique has been proposed in [34] so that all four methods yield the same high precision.

For the diffuse interface PB models [10–17], the trilinear approach is commonly used for approximating Dirac delta distributions. The development of regularization formulation is hindered by the fact that the fundamental solution with a space dependent dielectric function is unavailable. Recently, this difficulty has been resolved in [22] by conducting a dual decomposition for both potential and dielectric functions [35]. By splitting the dielectric profile into a constant base plus space changing part, the Coulomb component is defined with the constant dielectric coefficient, and can be captured analytically via Green's functions. The reaction field component then becomes bounded, and satisfies a regularized PB equation with a smooth source. This regularization method was validated by using the GCS model in [22], and is applicable to other diffuse interface PB models [10–17].

In this work, we will investigate the convergence of the GCS diffuse interface PB model to the sharp interface PB model. In particular, through analyzing the weak solutions for the regularized PB equations, we will rigorously prove that the reaction field potential in the regularization for the diffuse interface model converges to its counterpart for the sharp interface model. Convergence in electrostatic free energy will also be established. A numerical illustration of energy convergence for real molecular systems will be considered. However, the actual convergence cannot be realized computationally, because an infinitesimal mesh size has to be used. This is essentially why a theoretical proof is indispensable in diffuse interface implicit solvent modeling.

The theoretical convergence of diffuse interfaces to the sharp interface has been examined in other type of PB models. In [15], the convergence of a phase-field variational model defined via the Van der Waals-Cahn-Hilliard functional to its sharp interface limit is studied. The Γ-convergence of the phase-field free energy functionals to their sharp interface limit has been proved, together with the convergence of potential solution and dielectric boundary force. In [17], a diffuse interface energy functional is constructed by using a characteristic function representing the volume ratio of the solute in the solvent-solute transition region. Then, as the width of the transition region tends to zero, the convergences of the electrostatic potential and free energy to the sharp interface ones have been studied.

We note that the above theoretical studies [15,17] concern with the convergence in the potential by means of a trilinear approach. Driven by the popularity of the regularization in the implicit solvent simulations, the present study investigates the convergence of the reaction field potential in the presence of singular sources. In fact, this work unifies the regularization formulation for both sharp and diffuse interface PB models, which could provide a theoretical foundation for formulating regularization of more complicated problems, such as the Gaussian and super-Gaussian PB models with heterogeneous dielectric distributions [18,20]. Therefore, the insight revealed in our theoretical study will play an important role in future development of the PB model and its regularization.

The rest of this paper is organized as follows. We will first establish notations at the end of this section. In Section 2, we first review the diffuse interface and sharp interface PB models and their regularization. We then present our convergence analysis and the main theorems. Numerical study on several molecular systems will be considered in Section 3, together with a discussion on molecular surfaces. Finally, this paper ends with a conclusion.

Notations: Given $1 \le p \le \infty$ and $m \in \mathbb{N}$, $L^p(\Omega;\mathbb{R}^m)$ denotes the set of all p-integrable (Lebesgue) measurable functions defined on Ω taking value in $\mathbb{R}^m$. We denote its norm by $\|\cdot\|_{L^p(\Omega)}$. $W^{k,p}(\Omega;\mathbb{R}^m)$ stands for the Sobolev space consisting of functions whose weak derivatives up to kth order belong to $L^p(\Omega;\mathbb{R}^m)$. Additionally, $H^k(\Omega;\mathbb{R}^m) = W^{k,2}(\Omega;\mathbb{R}^m)$ for $k \in \mathbb{N}$, whose norm is denoted by $\|\cdot\|_{H^k(\Omega)}$. $W_0^{k,p}(\Omega;\mathbb{R}^m)$ and $H_0^k(\Omega;\mathbb{R}^m)$ stand for the closures of $C_0^\infty(\Omega;\mathbb{R}^m)$ in $W^{k,p}(\Omega;\mathbb{R}^m)$ and $H^k(\Omega;\mathbb{R}^m)$, respectively. When $m = 1$, we abbreviate the notations to $L^p(\Omega)$, $W^{k,p}(\Omega)$, $W_0^{k,p}(\Omega)$, $H^k(\Omega)$ and $H_0^k(\Omega)$, respectively. In addition, $H^{-1}(\Omega)$ is the dual space of $H_0^1(\Omega)$ with respect to the inner product in L^2.

In this article, $\mathbf{r} = (x, y, z)$ denotes the coordinates in $\mathbb{R}^3$. For any two open subsets $U, V \subset \mathbb{R}^3$, $V \subset\subset U$ means that $\overline{V} \subset U$. Given any two Banach spaces X, Y, the notations

$$X \hookrightarrow Y, \qquad X \overset{c}{\hookrightarrow} Y$$

mean that X is continuously and further compactly embedded into Y, respectively. Given a sequence $\{u_k\}_{k=1}^\infty = (u_1, u_2, \ldots)$ in X, $u_k \rightharpoonup u$ in X means that u_k converge weakly to some $u \in X$.

2. Mathematical modeling and analysis

In this section, we will first review the sharp and diffuse interface PB models, and discuss the corresponding regularization and weak solutions. Then, we will prove the convergence of the reaction-field potential and electrostatic free energy.

2.1. The sharp interface PB model

Consider a 3-dimensional solute-solvent system contained in a bounded Lipschitz domain $\Omega \subset \mathbb{R}^3$ satisfying a uniform exterior ball condition, which is fulfilled by any bounded C^2 domain; see [36, Exercise 2.11] for example. We further assume that Ω is composed of two disjoint subdomains with Lipschitz boundaries:

- Ω_m: inner solute (molecular) region, and
- Ω_s: outer solvent region,

i.e. $\Omega = \Omega_m \cup \Gamma \cup \Omega_s$, where $\Gamma = \partial\Omega_m \cap \partial\Omega_s$ is the solute-solvent interface. Denote by $\partial\Omega$ the boundary of Ω. Assume that the solute region Ω_m contains N_m solute atoms centered at $\mathbf{r}_1, \ldots, \mathbf{r}_{N_m}$. Characteristic functions χ_{Ω_s} and χ_{Ω_m} will be used to identify solvent and solute subdomains, respectively. For instance, $\chi_{\Omega_s}(\mathbf{r}) = 1$ when $\mathbf{r} \in \Omega_s$ and $\chi_{\Omega_s}(\mathbf{r}) = 0$ otherwise.

In the PB model [1–3], charges in Ω_m are partial charges assigned to the centers of atoms by using force fields, while charges in Ω_s are mobile ions described by the Boltzmann distribution. Applying Gauss's law to the charge distribution in both Ω_m and Ω_s, then the electrostatic potential u of the solute-solvent system is governed by the PB equation in the dimensionless form Holst [4]

$$\begin{cases} -\nabla\cdot(\epsilon\nabla u) + \chi_{\Omega_s}\kappa^2 \sinh u = \rho & \text{in} \quad \Omega; \\ u = u_b & \text{on} \quad \partial\Omega, \end{cases} \tag{2.1}$$

where the dielectric constant is defined by

$$\epsilon = \epsilon_m \chi_{\Omega_m} + \epsilon_s \chi_{\Omega_s},$$

with ϵ_m and ϵ_s being dielectric constant, respectively, for the molecule and water. Here the source term is due to singular charges contained in the protein

$$\rho(\mathbf{r}) = 4\pi \frac{e_c^2}{k_B T} \sum_{j=1}^{N_m} q_j \delta(\mathbf{r} - \mathbf{r}_j), \quad \text{in } \Omega, \tag{2.2}$$

where N_m is the total number of atoms in the solute molecule, k_B is the Boltzmann constant, and T is the absolute temperature. For each atom, a partial charge q_j in terms of the fundamental charge e_c is located at the atom center $\mathbf{r}_j$. The modified Debye-Hückel parameter κ takes a constant value

$$\kappa^2 = \left(\frac{2N_A e_c^2}{100 k_B T}\right) I = 8.486902807 \mathring{A}^{-2} I,$$

where N_A is the Avogadro's Number and I is the molar ionic strength. The boundary condition can be written as

$$u_b(\mathbf{r}) = \frac{e_c^2}{k_B T} \sum_{j=1}^{N_m} \frac{q_j}{\epsilon_s |\mathbf{r} - \mathbf{r}_j|} e^{-|\mathbf{r}-\mathbf{r}_j|\sqrt{\frac{\kappa^2}{\epsilon_e}}}, \quad \text{on } \partial\Omega. \tag{2.3}$$

The singular source term of (2.1) is a well known difficulty in analysis and computation of the PB equation. To overcome the difficulty, a two-component regularization [8,23,27,34] will be employed. In particular, we decompose the solution, u_Γ, of (2.1) into two parts:

$$u_\Gamma = \tilde{u}_\Gamma + u_C,$$

where $\tilde{u}_\Gamma$ and u_C are reaction field potential and Coulomb potential, respectively. The Coulomb potential u_C captures the singularities by means of

$$\begin{cases} -\epsilon_m \Delta u_C = \rho & \text{in} \quad \mathbb{R}^3; \\ u_C(\mathbf{r}) \to 0 & \text{as} \quad |\mathbf{r}| \to \infty. \end{cases} \tag{2.4}$$

The solution to the above equation is given analytically by the Green's function

$$u_C(\mathbf{r}) = G(\mathbf{r}) = \frac{e_c^2}{k_B T} \sum_{j=1}^{N_m} \frac{q_j}{\epsilon_m |\mathbf{r} - \mathbf{r}_j|}.$$

It is well known that

$$G \in C^\infty(\mathbb{R}^3 \setminus \{\mathbf{r}_1, \ldots, \mathbf{r}_{N_m}\}).$$

For the present sharp interface PB model, we apply the dual decomposition idea originally developed for the diffuse interface PB model [22]. In particular, we will decompose the dielectric function as $\epsilon = \hat{\epsilon} + \epsilon_m$. Then we expect that the reaction field potential $\tilde{u}_\Gamma$ solves

$$\begin{cases} -\nabla \cdot (\epsilon \nabla u) + \chi_{\Omega_s} \kappa^2 \sinh(u + u_C) = \nabla \cdot (\hat{\epsilon} \nabla u_C) & \text{in} \quad \Omega; \\ u = u_b - u_C & \text{on} \quad \partial\Omega. \end{cases} \tag{2.5}$$

A key observation is that despite of the singularities of u_C inside Ω_m, the coefficients χ_{Ω_s} and $\hat{\epsilon}$ vanish in Ω_m. As a direct consequence, (2.5) is a well-defined nonlinear second order elliptic problem and the singularities of the solution u are captured by those of the Green's function u_C. For this reason, (2.5) is usually termed the regularized Poisson-Boltzmann (RPB) equation. The term $\nabla \cdot (\hat{\epsilon} \nabla u_C) \in H^{-1}(\Omega)$ and thus, for any $\phi \in C_0^1(\Omega)$, we have

$$\int_\Omega \nabla \cdot (\hat{\epsilon} \nabla u_C) \phi \, d\mathbf{r} = -\int_\Omega \hat{\epsilon} \nabla u_C \cdot \nabla \phi \, d\mathbf{r}.$$

This motivates the following definition of weak solutions.

Definition 2.1. Consider the following Dirichlet problem of the semilinear strictly elliptic equation

$$\begin{cases} -\nabla \cdot (a \nabla u) + F(\mathbf{r}, u) = \nabla \cdot f & \text{in} \quad \Omega; \\ u = g & \text{on} \quad \partial\Omega. \end{cases} \tag{2.6}$$

Suppose that

$$a \in L^\infty(\Omega), \quad f \in L^2(\Omega; \mathbb{R}^3), \quad g \in L^2(\partial\Omega)$$

and $F(\cdot, \cdot)$ is measurable in $\Omega \times \mathbb{R}$,

$$F(\mathbf{r}, \cdot) \in C^{1-}(\mathbb{R}), \quad \forall \mathbf{r} \in \Omega,$$

where $C^{1-}(\mathbb{R})$ denotes the set of Lipschitz continuous functions on $\mathbb{R}$; and for any $M > 0$, $F(\mathbf{r}, s)$ is uniformly bounded for $(\mathbf{r}, s) \in \Omega \times [-M, M]$. Then we call $u \in H^1(\Omega) \cap L^\infty(\Omega)$ a weak solution to (2.6) if for any $\phi \in C_0^\infty(\Omega)$

$$\int_\Omega [a(\mathbf{r}) \nabla u(\mathbf{r}) \cdot \nabla \phi(\mathbf{r}) + F(\mathbf{r}, u) \phi(\mathbf{r}) + f(\mathbf{r}) \cdot \nabla \phi(\mathbf{r})] \, d\mathbf{r} = 0 \tag{2.7}$$

and

$$u = g \quad \text{on } \partial\Omega$$

in the trace sense.

It follows from [23, Theorems 4.5 and 5.1] that (2.5) has a weak solution $\widetilde{u}_\Gamma$, that is, $\widetilde{u}_\Gamma \in H^1(\Omega) \cap L^\infty(\Omega)$ with boundary trace $u_b - u_C$ and for any $\phi \in C_0^\infty(\Omega)$

$$\int_\Omega \left[\epsilon \nabla \widetilde{u}_\Gamma \cdot \nabla \phi + \chi_{\Omega_s} \kappa^2 \sinh(\widetilde{u}_\Gamma + u_C)\phi + \hat{\epsilon} \nabla u_C \cdot \nabla \phi\right] d\mathbf{r} = 0$$

by the above definition.

Remark 2.2. The difference between the present RPB Eq. (2.5) and that of the two-component regularization [23,27] is the source term $\nabla \cdot (\hat{\epsilon} \nabla u_C)$. We note that $\nabla \cdot (\hat{\epsilon} \nabla u_C)$ is a Radon measure supported only on Γ. In particular, following [34], $\nabla \cdot (\hat{\epsilon} \nabla u_C)$ can be rewritten as

$$\begin{cases} \nabla \cdot (\hat{\epsilon} \nabla u_C) = (\epsilon_m - \epsilon_m)\Delta u_C = 0, & \text{in } \Omega_m \\ \nabla \cdot (\hat{\epsilon} \nabla u_C) = (\epsilon_s - \epsilon_m)\Delta u_C = (\epsilon_s - \epsilon_m)\Delta G, & \text{in } \Omega_s \\ [u_C] = u_C^+ - u_C^- = 0, & \text{on } \Gamma \\ \left[\hat{\epsilon} \frac{\partial u_C}{\partial n}\right] = \hat{\epsilon}^+ \frac{\partial u_C^+}{\partial n} - \hat{\epsilon}^- \frac{\partial u_C^-}{\partial n} = (\epsilon_s - \epsilon_m) \frac{\partial G}{\partial n}, & \text{on } \Gamma \\ u_C = G, & \text{on } \partial\Omega. \end{cases} \tag{2.8}$$

Since ΔG is vanishing in Ω_s, this source term is omitted in [23,27]. However, as pointed out in [34], the negligence of such a source term will introduce a noticeable approximation error. Thus, in order to recover the accuracy, such a source term should be kept in the numerical discretization. In fact, by keeping a source term which is essentially equivalent to the present one [34], the two-component regularization [23,27] yields the same high precision as the regularized Matched Interface and Boundary (rMIB) method [8,29]. Therefore, instead of implementing the source term $\nabla \cdot (\hat{\epsilon} \nabla u_C)$ by means of (2.8), the existing rMIB package [8] will be employed, for simplicity, to demonstrate the regularization of the sharp interface PB equation.

2.2. A Diffuse Interface PB model

Following the ideas in [22], we will introduce a family of diffuse interface PB models with smooth solute-solvent boundaries. The solute-solvent boundary is constructed by using a smeared surface function S. Let U_1 and U_2 be two open Lipschitz subsets of Ω satisfying

$$U_1 \subset\subset \Omega_m \subset\subset U_2 \subset\subset \Omega \quad \text{and} \quad \{\mathbf{r}_1, \ldots, \mathbf{r}_{N_m}\} \subset U_1. \tag{2.9}$$

Recall that, for any two open subsets $U, V \subset \mathbb{R}^3$, $V \subset\subset U$ means that $\overline{V} \subset U$. A smeared surface function $S : \Omega \to [0, 1]$ is a C^2-function with the following properties:

(S1) $S(\mathbf{r}) = 1$ for all $\mathbf{r} \in U_1$, and
(S2) $S(\mathbf{r}) = 0$ for all $\mathbf{r} \in \Omega \setminus \overline{U}_2$.

Then the diffuse dielectric coefficient ϵ_d is given by

$$\epsilon_d(\mathbf{r}) = \epsilon_m S(\mathbf{r}) + \epsilon_s[1 - S(\mathbf{r})].$$

For the present setting, the electrostatic potential u is determined by the following diffuse interface PB problem [22]

$$\begin{cases} -\nabla \cdot (\epsilon_d \nabla u) + (1 - S)\kappa^2 \sinh u = \rho & \text{in } \Omega; \\ u = u_b & \text{on } \partial\Omega. \end{cases} \tag{2.10}$$

The regularization of the diffuse interface PB equation has been successfully formulated in [22], by conducting a dual decomposition of potential and dielectric function. In particular, we can decompose ϵ_d into

$$\epsilon_d = \epsilon_m + \hat{\epsilon}_d \quad \text{with} \quad \hat{\epsilon}_d = (\epsilon_s - \epsilon_m)(1 - S).$$

We denote the solution to (2.10) by u_d, which can be decomposed into

$$u_d = \widetilde{u}_d + u_C.$$

Proposition 2.3. *The reaction field potential $\widetilde{u}_d$ is the unique weak solution of*

$$\begin{cases} -\nabla \cdot (\epsilon_d \nabla u) + (1 - S)\kappa^2 \sinh(u + u_C) = \nabla \cdot (\hat{\epsilon}_d \nabla u_C) & \text{in } \Omega; \\ u = u_b - u_C & \text{on } \partial\Omega. \end{cases} \tag{2.11}$$

Proof. Let us further introduce a three-component decomposition of $\widetilde{u}_d$. We first consider

$$\begin{cases} \Delta H = 0 & \text{in } \Omega; \\ H = u_b - u_C & \text{on } \partial\Omega. \end{cases} \tag{2.12}$$

Extend $(u_b - u_C)|_{\partial\Omega}$ to be a function $f \in C^\infty(\overline{\Omega})$ by possibly multiplying $u_b - u_C$ by a smooth cut-off function to remove the singularities. Then $\widetilde{H} := H - f$ solves

$$\begin{cases} \Delta\widetilde{H} &= \Delta f \quad \text{in} \quad \Omega; \\ \widetilde{H} &= 0 \quad \text{on} \quad \partial\Omega. \end{cases} \tag{2.13}$$

It follows from [37, Corollary 1 and the remark on Page 9] that $\widetilde{H} \in H^2(\Omega) \cap H_0^1(\Omega)$. We put $u_{BC} = u_C + H$. Then

$$\begin{cases} -\epsilon_m \Delta u_{BC} &= \rho \quad \text{in} \quad \Omega; \\ u_{BC} &= u_b \quad \text{on} \quad \partial\Omega. \end{cases} \tag{2.14}$$

It is worthwhile to point out that u_{BC} is independent of the smeared surface function S. Moreover, by the Sobolev embeddings

$H^2(\Omega) \hookrightarrow W^{1,6}(\Omega) \hookrightarrow C(\overline{\Omega})$,

it holds that

$$\|u_{BC}\|_{L^\infty(\Omega\setminus U_1)} + \|\nabla u_{BC}\|_{L^6(\Omega\setminus U_1)} < M_1 \tag{2.15}$$

for some $M_1 > 0$ independent of S. This is a crucial estimate in the proof of the convergence theorem, Theorem 2.6, in the next subsection.

Subtracting u_{BC} from u_d motivates us to consider the weak solution, $u_{\mathrm{R},d}$, of

$$\begin{cases} -\nabla\cdot(\epsilon_d\nabla u) + (1-S)\kappa^2\sinh(u+u_{BC}) &= \nabla\cdot(\hat{\epsilon}_d\nabla u_{BC}) \quad \text{in} \quad \Omega; \\ u &= 0 \quad \text{on} \quad \partial\Omega. \end{cases} \tag{2.16}$$

We can introduce a further decomposition $u_{\mathrm{R},d} = u_{L,d} + u_{N,d}$ in such a way that $u_{L,d}$ solves

$$\begin{cases} -\nabla\cdot(\epsilon_d\nabla u) &= \nabla\cdot(\hat{\epsilon}_d\nabla u_{BC}) \quad \text{in} \quad \Omega; \\ u &= 0 \quad \text{on} \quad \partial\Omega, \end{cases} \tag{2.17}$$

and $u_{N,d}$ solves

$$\begin{cases} -\nabla\cdot(\epsilon_d\nabla u) + (1-S)\kappa^2\sinh(u+u_{BC}+u_{L,d}) &= 0 \quad \text{in} \quad \Omega; \\ u &= 0 \quad \text{on} \quad \partial\Omega. \end{cases} \tag{2.18}$$

The existence and uniqueness of a weak solution to the Dirichlet problem (2.17) is an immediate result of the standard elliptic theory, cf. [36, Theorems 8.3 and 8.16]. Observe that $\hat{\epsilon}_d(\mathbf{r}) = 0$ for all $\mathbf{r} \in U_1$. Therefore, we have a unique weak solution $u_{L,d}$ to (2.17) with

$$\|u_{L,d}\|_{L^\infty(\Omega)} \le \widehat{M} \quad \text{for some } \widehat{M} > 0.$$

To study (2.18), we consider the energy functional defined by

$$I_d[u] = \int_\Omega \left[\frac{\epsilon_d}{2}|\nabla u|^2 + (1-S)\kappa^2\cosh(u_{BC}+u_{L,d}+u)\right] d\mathbf{r}, \quad u \in H_0^1(\Omega).$$

The existence of a minimizer $I_d[u_{N,d}] = \min_{u\in H_0^1(\Omega)} I_d[u]$ follows from the direct method of Calculus of Variation. Note that $u_{N,d}$ weakly solves (2.18) if and only if it is a critical point of $I_d[\cdot]$ that further belongs to $L^\infty(\Omega)$. The uniqueness of a critical point of the functional $I_d[\cdot]$ is an immediate consequence of its strict convexity. We will show that $u_{N,d} \in L^\infty(\Omega)$.

Define

$$W = \{\mathbf{r} \in \Omega : u_{N,d}(\mathbf{r}) \ge M_1 + \widehat{M}\}.$$

Multiplying both sides of (2.18) by $(u_{N,d} - M_1 - \widehat{M})_+$ and integrating over Ω yields

$$\int_W \left[\epsilon_d|\nabla u_{N,d}|^2 + (1-S)\kappa^2\sinh(u_{N,d}+u_{BC}+u_{L,d})(u_{N,d}-M_1-\widehat{M})_+\right] d\mathbf{r} = 0.$$

Because both terms in the integrand are non-negative, this implies that

$$u_{N,d} \le M_1 + \widehat{M} \quad \text{a.e. on } \Omega\setminus U_1.$$

Similarly, we can show that

$$u_{N,d} \ge -M_1 - \widehat{M} \quad \text{a.e. on } \Omega\setminus U_1.$$

Combining the above estimates with [36, Theorem 8.16], we have proved that

$$\|u_{N,d}\|_{L^\infty(\Omega)} \le \widetilde{M} \quad \text{for some } \widetilde{M} > 0. \tag{2.19}$$

Therefore, $u_{N,d}$ is indeed a weak solution of (2.18).

We have thus obtained a weak solution $\widetilde{u}_d = H + u_{L,d} + u_{N,d}$ to (2.11). By our construction, $\widetilde{u}_d$ is the unique weak solution to (2.11). □

Remark 2.4. A few remarks are in order.

(1) The three-component decomposition $\widetilde{u}_d = H + u_{L,d} + u_{N,d}$ seems to be excessively complex. However, this decomposition turns out to be useful in the proof of the convergence theorem, Theorem 2.6.

(2) In contrast with the discontinuity of $\nabla\widetilde{u}_\Gamma$ across Γ, in the diffuse interface PB Eq. (2.10), the gradient of the reaction field potential is continuous throughout Ω. Indeed, applying [36, Theorem 8.10] to (2.11), one can show that $\widetilde{u}_d \in W^{3,2}(\Omega')$ for any subdomain $\Omega' \subset\subset \Omega$. Then the assertion follows from the Sobolev embedding theorem.

2.3. Convergence

Arguably, sharp interface models are the most popular type of interface model in the mathematical analysis of multiphase problems. One possible explanation is that the extensive research on the sharp interface based transmission problems and free boundary problems lay the solid foundation for analyzing multiphase problems. In the study of implicit solvation, diffuse interface PB models are nevertheless the more physical choice, as discussed in the introduction. It is a natural question to ask whether they are analytically reasonable generalizations of the sharp interface PB model. To this end, we will study the convergence of the electrostatic potentials and free energies of diffuse interface PB models to their sharp interface counterparts.

Take a sequence of smeared surface functions $S_n : \Omega \to [0, 1]$ satisfying, in addition,

(S0) $S_n \to \chi_{\Omega_m}$ in $L^1(\Omega)$ as $n \to \infty$.

Then the sharp interface dielectric coefficient ϵ can be approximated by the diffuse ones

$$\epsilon_n(\mathbf{r}) = \epsilon_m S_n(\mathbf{r}) + \epsilon_s[1 - S_n(\mathbf{r})]$$

in $L^1(\Omega)$. Observe that S_n and thus ϵ_n are uniformly bounded in $L^\infty(\Omega)$. Therefore, the Riesz-Thorin interpolation theorem implies that

$$\lim_{n\to\infty} \|\epsilon_n - \epsilon\|_{L^r(\Omega)} = 0, \quad r \in [1, \infty). \tag{2.20}$$

Example 2.5. Consider the 3-dimensional Gaussian kernel

$$K_\sigma(\mathbf{r}) = \frac{1}{\left(\sigma\sqrt{2}\right)^3} \exp\left(-\frac{|\mathbf{r}|^2}{2\sigma^2}\right), \quad \sigma > 0.$$

Given an arbitrary positive sequence $\{\sigma_n\}_{n=1}^\infty$ with limit 0, put

$$\widetilde{S}_n(\mathbf{r}) = \chi_{\Omega_m} * K_{\sigma_n}(\mathbf{r}) = \int_{\Omega_m} K_{\sigma_n}(\mathbf{r} - \mathbf{r}')\, d\mathbf{r}'.$$

It is well known that

$$\widetilde{S}_n \to \chi_{\Omega_m} \quad \text{in } L^1(\Omega).$$

Pick two smooth cut-off functions $\phi, \psi : \Omega \to [0, 1]$ such that

$$\phi(\mathbf{r}) = \begin{cases} 1, & \text{when } \mathbf{r} \in \Omega_m, \\ 0, & \text{when } \mathbf{r} \in \Omega \setminus \overline{U}_2, \end{cases}$$

and

$$\psi(\mathbf{r}) = \begin{cases} 1, & \text{when } \mathbf{r} \in U_1, \\ 0, & \text{when } \mathbf{r} \in \Omega \setminus \overline{\Omega}_m. \end{cases}$$

Now we define

$$S_n(\mathbf{r}) = \phi(\mathbf{r})\big[\psi(\mathbf{r}) + (1 - \psi(\mathbf{r}))\widetilde{S}_n(\mathbf{r})\big].$$

Note that $\chi_{\Omega_m}(\mathbf{r}) = \phi(\mathbf{r})\big[\psi(\mathbf{r}) + (1 - \psi(\mathbf{r}))\chi_{\Omega_m}(\mathbf{r})\big]$. Direct computations show that

$$\begin{aligned} \int_\Omega |S_n(\mathbf{r}) - \chi_{\Omega_m}(\mathbf{r})|\, d\mathbf{r} &\le \int_\Omega \phi(\mathbf{r})(1 - \psi(\mathbf{r}))\big|\widetilde{S}_n(\mathbf{r}) - \chi_{\Omega_m}(\mathbf{r})\big|\, d\mathbf{r} \\ &\le \int_\Omega \big|\widetilde{S}_n(\mathbf{r}) - \chi_{\Omega_m}(\mathbf{r})\big|\, d\mathbf{r}. \end{aligned}$$

Therefore, the sequence $\{S_n\}_{n=1}^\infty$ satisfies Conditions (S0)-(S2). $\{S_n\}_{n=1}^\infty$ are exactly the Gaussian convolution surface (GCS) functions with convolution parameter $\{\sigma_n\}_{n=1}^\infty$, cf. [22].

A unified regularization formulation is considered as in the sharp interface PB model. As in Sections 2.1 and 2.2, we rewrite the approximating dielectric coefficients ϵ_n as

$$\epsilon_n = \epsilon_m + \hat{\epsilon}_n \quad \text{with} \quad \hat{\epsilon}_n = (\epsilon_s - \epsilon_m)(1 - S_n),$$

and decompose the solution u_n of

$$\begin{cases} -\nabla \cdot (\epsilon_n \nabla u) + (1 - S_n)\kappa^2 \sinh u = \rho & \text{in} \quad \Omega; \\ u = u_b & \text{on} \quad \partial\Omega \end{cases} \tag{2.21}$$

into [22]

$$u_n = \widetilde{u}_n + u_C.$$

By Proposition 2.3, $\widetilde{u}_n$ is the unique weak solution of

$$\begin{cases} -\nabla \cdot (\epsilon_n \nabla u) + (1 - S_n)\kappa^2 \sinh(u + u_C) = \nabla \cdot (\hat{\epsilon}_n \nabla u_C) & \text{in} \quad \Omega; \\ u = u_b - u_C & \text{on} \quad \partial\Omega. \end{cases} \tag{2.22}$$

We note that the RPB Eq. (2.22) is basically the one proposed in [22]. Because the source term $\nabla \cdot (\hat{\epsilon}_n \nabla u_C)$ is smooth and bounded, the standard finite difference is sufficient for solving the diffuse interface PB equation numerically, which is much simpler than the rMIB algorithm for the sharp interface PB equation [8,29,34]. In the present study, the finite difference solver developed in [22] will be used to demonstrate the regularization of the diffuse interface PB model.

Theorem 2.6. *For each n, (2.21) has a unique solution of the form $u_n = \widetilde{u}_n + u_C$, where $\widetilde{u}_n$ is the unique weak solution of (2.22). Moreover,*

$$\|u_n - u_\Gamma\|_{H^1(\Omega)} \to 0 \quad \text{as } n \to \infty,$$

or equivalently,

$$\widetilde{u}_n \to \widetilde{u}_\Gamma \quad \text{in } H^1(\Omega) \quad \text{as } n \to \infty, \tag{2.23}$$

where $u_\Gamma = \widetilde{u}_\Gamma + u_C$ is the unique solution of (2.1) with $\widetilde{u}_\Gamma$ weakly solving (2.5).

Proof. The existence and uniqueness of weak solutions $u_n = \widetilde{u}_n + u_C$ of (2.21) is proved in Section 2.2.

To study the convergence (2.23), we will first show that

$$\widetilde{u}_n \to \widetilde{u}_\Gamma \quad \text{in } L^2(\Omega) \quad \text{as } n \to \infty. \tag{2.24}$$

Recall the definition of u_{BC}, which solves (2.14). Note that $\nabla \cdot [\hat{\epsilon}_n(\mathbf{r})\nabla u_{BC}(\mathbf{r})] = 0$ for all $\mathbf{r} \in U_1$ and the bound M_1 in (2.15) is independent of n.

As in the proof of Proposition 2.3, we consider the weak solution, $u_{\mathrm{R},n} = u_n - u_{BC}$, of

$$\begin{cases} -\nabla \cdot (\epsilon_n \nabla u) + (1 - S_n)\kappa^2 \sinh(u + u_{BC}) = \nabla \cdot (\hat{\epsilon}_n \nabla u_{BC}) & \text{in} \quad \Omega; \\ u = 0 & \text{on} \quad \partial\Omega, \end{cases} \tag{2.25}$$

and the weak solution, $u_{\mathrm{R},\Gamma} = u_\Gamma - u_{BC}$, of

$$\begin{cases} -\nabla \cdot (\epsilon \nabla u) + \chi_{\Omega_s}\kappa^2 \sinh(u + u_{BC}) = \nabla \cdot (\hat{\epsilon} \nabla u_{BC}) & \text{in} \quad \Omega; \\ u = 0 & \text{on} \quad \partial\Omega. \end{cases} \tag{2.26}$$

Given an arbitrary subsequence of $u_{\mathrm{R},n}$, not relabelled, we decompose them into $u_{\mathrm{R},n} = u_{L,n} + u_{N,n}$, where $u_{L,n}$ is the unique weak solution of

$$\begin{cases} -\nabla \cdot (\epsilon_n \nabla u) = \nabla \cdot (\hat{\epsilon}_n \nabla u_{BC}) & \text{in} \quad \Omega; \\ u = 0 & \text{on} \quad \partial\Omega, \end{cases} \tag{2.27}$$

and $u_{N,n}$ is the unique weak solution of

$$\begin{cases} -\nabla \cdot (\epsilon_n \nabla u) + (1 - S_n)\kappa^2 \sinh(u + u_{BC} + u_{L,n}) = 0 & \text{in} \quad \Omega; \\ u = 0 & \text{on} \quad \partial\Omega. \end{cases} \tag{2.28}$$

Note that $u_{L,n}$ is a valid test function in (2.7). Multiply both sides of (2.27) by $u_{L,n}$ and integrate over Ω. This yields

$$\int_\Omega \epsilon_n |\nabla u_{L,n}|^2 \, d\mathbf{r} \le \left| \int_\Omega \hat{\epsilon}_n \nabla u_{BC} \cdot \nabla u_{L,n} \right| d\mathbf{r}. \tag{2.29}$$

By the Hölder and Young's inequalities, the right hand side of (2.29) can be estimated as

$$\left| \int_\Omega \hat{\epsilon}_n \nabla u_{BC} \cdot \nabla u_{L,n} \, d\mathbf{r} \right| \le C \left| \int_{\Omega \setminus U_1} \nabla u_{BC} \cdot \nabla u_{L,n} \, d\mathbf{r} \right|$$

$$\leq L(\delta)\|\nabla u_{BC}\|^2_{L^2(\Omega\setminus U_1)} + \delta\|\nabla u_{L,n}\|^2_{L^2(\Omega)} \tag{2.30}$$

for any $\delta > 0$ and a continuous and decreasing function $L : \mathbb{R}_+ \to \mathbb{R}_+$.

Choosing $\delta > 0$ sufficiently small, we can infer from (2.15), (2.29), (2.30) and the Hölder and Poincaré's inequalities that

$$\|u_{L,n}\|_{H^1(\Omega)} < M_2 \tag{2.31}$$

for some constant $M_2 > 0$ uniform in n.

Note that $\hat{\epsilon}_n \nabla u_{BC}$ is uniformly bounded in $L^6(\Omega)$. We infer from [36, Theorem 8.16] that

$$\|u_{L,n}\|_{L^\infty(\Omega)} < M_3 \tag{2.32}$$

for some $M_3 > 0$ independent of n.

Applying a similar argument leading to (2.19), we obtain

$$\|u_{N,n}\|_{L^\infty(\Omega)} \leq M_4 \tag{2.33}$$

for some constant $M_4 > 0$ independent of n. Multiplying both sides of (2.28) by $u_{N,n}$ and integrating over Ω give

$$\int_\Omega \left[\epsilon_n |\nabla u_{N,n}|^2 + (1 - S_n)\kappa^2 \sinh(u_{N,n} + u_{BC} + u_{L,n})u_{N,n}\right] d\mathbf{r} = 0.$$

In view of (2.15), (2.32) and (2.33), we can again infer from the Poincaré inequality that

$$\|u_{N,n}\|_{H^1(\Omega)} < M_5 \tag{2.34}$$

for some constant $M_5 > 0$ independent of n. Combining (2.31) and (2.34), we thus have

$$\|u_{\mathrm{R},n}\|_{H^1(\Omega)} < M_2 + M_5. \tag{2.35}$$

Therefore, there exists some $u_{\mathrm{R},\Gamma} \in H^1_0(\Omega)$ such that up to a further subsequence, not relabelled,

$$u_{\mathrm{R},n} \to u_{\mathrm{R},\Gamma} \quad \text{in } L^2(\Omega) \quad \text{and} \quad u_{\mathrm{R},n} \rightharpoonup u_{\mathrm{R},\Gamma} \quad \text{in } H^1(\Omega). \tag{2.36}$$

Moreover,

$$\|u_{\mathrm{R},\Gamma}\|_{L^\infty(\Omega)} \leq \|u_{\mathrm{R},n}\|_{L^\infty(\Omega)} < M_3 + M_4. \tag{2.37}$$

Consider the weak formulation of (2.25), i.e. for any $\phi \in C^\infty_0(\Omega)$

$$\int_\Omega \left[\epsilon_n \nabla u_{\mathrm{R},n} \cdot \nabla\phi + \kappa^2(1 - S_n)\sinh(u_{BC} + u_{\mathrm{R},n})\phi + \hat{\epsilon}_n \nabla u_{BC} \cdot \nabla\phi\right] d\mathbf{r} = 0. \tag{2.38}$$

By the mean value theorem, (2.15), (2.32), (2.33) and (2.37), we have

$$\begin{aligned}
&\left|\int_\Omega \left[\kappa^2(1 - S_n)\sinh(u_{BC} + u_{\mathrm{R},n})\phi\right] d\mathbf{r} - \int_\Omega \left[\kappa^2 \chi_{\Omega_s} \sinh(u_{BC} + u_{\mathrm{R},\Gamma})\phi\right] d\mathbf{r}\right| \\
\leq& C\Big[\int_{\Omega\setminus U_1} (1 - S_n)|\sinh(u_{BC} + u_{\mathrm{R},n}) - \sinh(u_{BC} + u_{\mathrm{R},\Gamma})|\, d\mathbf{r} \\
&+ \int_{\Omega\setminus U_1} |(1 - S_n) - \chi_{\Omega_s}||\sinh(u_{BC} + u_{\mathrm{R},\Gamma})|\, d\mathbf{r}\Big] \\
\leq& C\int_{\Omega\setminus U_1} \Big[|u_{\mathrm{R},n} - u_{\mathrm{R},\Gamma}| + |(1 - S_n) - \chi_{\Omega_s}|\Big] d\mathbf{r} \longrightarrow 0
\end{aligned}$$

as $n \to \infty$. In view of (2.15), (2.20), (2.35) and (2.36), it is a simple task to verify that

$$\lim_{n\to\infty} \int_\Omega \epsilon_n \nabla u_{\mathrm{R},n} \cdot \nabla\phi\, d\mathbf{r} = \int_\Omega \epsilon \nabla u_{\mathrm{R},\Gamma} \cdot \nabla\phi\, d\mathbf{r}$$

and

$$\lim_{n\to\infty} \int_\Omega \hat{\epsilon}_n \nabla u_{BC} \cdot \nabla u_{\mathrm{R},n}\, d\mathbf{r} = \int_\Omega \hat{\epsilon} \nabla u_{BC} \cdot \nabla u_{\mathrm{R},\Gamma}\, d\mathbf{r}. \tag{2.39}$$

Hence we can push $n \to \infty$ in (2.38) and obtain

$$\int_\Omega \left[\epsilon \nabla u_{\mathrm{R},\Gamma} \cdot \nabla\phi + \kappa^2 \chi_{\Omega_s} \sinh(u_{BC} + u_{\mathrm{R},\Gamma})\phi + \hat{\epsilon} \nabla u_{BC} \cdot \nabla\phi\right] d\mathbf{r} = 0. \tag{2.40}$$

Therefore, $u_{\mathrm{R},\Gamma}$ is a weak solution to (2.26).

Next, we will prove that

$$\lim_{n\to\infty} \int_\Omega \epsilon_n |\nabla u_n - \nabla u|^2\, d\mathbf{r} = 0,$$

or equivalently,

$$\lim_{n\to\infty}\int_\Omega \epsilon_n|\nabla u_{\mathrm{R},n}-\nabla u_{\mathrm{R},\Gamma}|^2\,d\mathbf{r}=0. \tag{2.41}$$

Since $C_0^\infty(\Omega)$ is dense in $H_0^1(\Omega)$, $\phi=u_{\mathrm{R},n}$ is a valid test function in (2.38). We consider

$$\begin{aligned}&\int_\Omega \epsilon_n|\nabla u_{\mathrm{R},n}|^2\,d\mathbf{r}\\ &=-\kappa^2\int_\Omega(1-S_n)\sinh(u_{BC}+u_{\mathrm{R},n})u_{\mathrm{R},n}\,d\mathbf{r}-\int_\Omega\hat{\epsilon}_n\nabla u_{BC}\cdot\nabla u_{\mathrm{R},n}\,d\mathbf{r}.\end{aligned} \tag{2.42}$$

To study the first term on the right hand side of (2.42), one can compute that

$$\begin{aligned}&\left|\int_\Omega(1-S_n)\sinh(u_{BC}+u_{\mathrm{R},n})u_{\mathrm{R},n}\,d\mathbf{r}-\int_\Omega\chi_{\Omega_s}\sinh(u_{BC}+u_{\mathrm{R},\Gamma})u_{\mathrm{R},\Gamma}\,d\mathbf{r}\right|\\ \le&\left|\int_\Omega[(1-S_n)-\chi_{\Omega_s}]\sinh(u_{BC}+u_{\mathrm{R},n})u_{\mathrm{R},n}\,d\mathbf{r}\right|\\ &+\left|\int_{\Omega_s}[\sinh(u_{BC}+u_{\mathrm{R},n})-\sinh(u_{BC}+u_{\mathrm{R},\Gamma})]u_{\mathrm{R},n}\,d\mathbf{r}\right|\\ &+\left|\int_{\Omega_s}\sinh(u_{BC}+u_{\mathrm{R},\Gamma})(u_{\mathrm{R},n}-u_{\mathrm{R},\Gamma})\,d\mathbf{r}\right|.\end{aligned}$$

By (2.15) and (2.37),

$$\lim_{n\to\infty}\left|\int_\Omega[(1-S_n)-\chi_{\Omega_s}]\sinh(u_{BC}+u_{\mathrm{R},n})u_{\mathrm{R},n}\,d\mathbf{r}\right|=0.$$

Similarly, by means of the mean value theorem, (2.15), (2.36) and (2.37), one can show that

$$\lim_{n\to\infty}\left|\int_{\Omega_s}[\sinh(u_{BC}+u_{\mathrm{R},n})-\sinh(u_{BC}+u_{\mathrm{R},\Gamma})]u_{\mathrm{R},n}\,d\mathbf{r}\right|=0$$

and

$$\lim_{n\to\infty}\left|\int_{\Omega_s}\sinh(u_{BC}+u_{\mathrm{R},\Gamma})(u_{\mathrm{R},n}-u_{\mathrm{R},\Gamma})\,d\mathbf{r}\right|=0.$$

Combining with (2.39) and (2.40), the above estimates imply that

$$\lim_{n\to\infty}\int_\Omega\epsilon_n|\nabla u_{\mathrm{R},n}|^2\,d\mathbf{r}=\int_\Omega\epsilon|\nabla u_{\mathrm{R},\Gamma}|^2\,d\mathbf{r}.$$

On the other hand, by the dominated convergence theorem,

$$\lim_{n\to\infty}\int_\Omega\epsilon_n|\nabla u_{\mathrm{R},\Gamma}|^2\,d\mathbf{r}=\int_\Omega\epsilon|\nabla u_{\mathrm{R},\Gamma}|^2\,d\mathbf{r}.$$

Now it follows that

$$\begin{aligned}&\lim_{n\to\infty}\int_\Omega\epsilon_n|\nabla u_{\mathrm{R},n}-\nabla u_{\mathrm{R},\Gamma}|^2\,d\mathbf{r}\\ &=\lim_{n\to\infty}\int_\Omega\left[\epsilon_n|\nabla u_{\mathrm{R},n}|^2-2\epsilon_n\nabla u_{\mathrm{R},n}\cdot\nabla u_{\mathrm{R},\Gamma}+\epsilon_n|\nabla u_{\mathrm{R},\Gamma}|^2\right]d\mathbf{r}\\ &=\int_\Omega\left[\epsilon|\nabla u_{\mathrm{R},\Gamma}|^2-2\epsilon\nabla u_{\mathrm{R},\Gamma}\cdot\nabla u_{\mathrm{R},\Gamma}+\epsilon|\nabla u_{\mathrm{R},\Gamma}|^2\right]d\mathbf{r}=0.\end{aligned}$$

By the Poincaré inequality, this proves (2.23).

It remains to show that $u_\Gamma=u_{\mathrm{R},\Gamma}+u_{BC}$ is the unique solution of (2.1), or equivalently, $u_{\mathrm{R},\Gamma}$ is the unique weak solution to (2.26). This follows from an analogous argument to the uniqueness part in the proof of Proposition 2.3. □

The energy released when the solute molecule is dissolved in the solvent is known as the free energy of solvation. The polar component of solvation free energy can be calculated in the linearized PB model by computing the difference between the total electrostatic free energy of the macromolecule in the solvent and in the vacuum. Therefore, the polar solvation energy can be calculated as [3]

$$E=\frac{1}{2}k_BT\int_\Omega\sum_{j=1}^{N_m}q_j\delta(\mathbf{r}-\mathbf{r}_j)[u_\Gamma(\mathbf{r})-u_C(\mathbf{r})]\,d\mathbf{r},$$

where u_Γ is the solution of (2.1). Similarly, we can define the approximating polar solvation energy as

$$E_n = \frac{1}{2}k_B T \int_\Omega \sum_{j=1}^{N_m} q_j \delta(\mathbf{r}-\mathbf{r}_j)[u_n(\mathbf{r}) - u_C(\mathbf{r})]\, d\mathbf{r}$$

for the solution u_n of (2.21).

Theorem 2.7. $\lim_{n\to\infty} E_n = E$.

Proof. Recall the decompositions $u_\Gamma = u_C + H + u_{\mathrm{R},\Gamma}$ and $u_n = u_C + H + u_{\mathrm{R},n}$. It clearly holds that

$$E = \frac{1}{2}k_B T \sum_{j=1}^{N_m} q_j H(\mathbf{r}_j) + \frac{1}{2}k_B T \int_\Omega \sum_{j=1}^{N_m} q_j \delta(\mathbf{r}-\mathbf{r}_j) u_{\mathrm{R},\Gamma}(\mathbf{r})\, d\mathbf{r}, \tag{2.43}$$

and

$$E_n = \frac{1}{2}k_B T \sum_{j=1}^{N_m} q_j H(\mathbf{r}_j) + \frac{1}{2}k_B T \int_\Omega \sum_{j=1}^{N_m} q_j \delta(\mathbf{r}-\mathbf{r}_j) u_{\mathrm{R},n}(\mathbf{r})\, d\mathbf{r}. \tag{2.44}$$

We will prove that $u_{\mathrm{R},\Gamma}$ and $u_{\mathrm{R},n}$ are indeed continuous in a neighbourhood of $\{\mathbf{r}_1,\dots,\mathbf{r}_{N_m}\}$ and thus the integrals in (2.43) and (2.44) are well-defined.

Observe that both $(1-S_n)$ and $\hat{\epsilon}_n$ are identically zero in U_1. We can thus infer from (2.25) that

$$\Delta u_{\mathrm{R},n} = 0 \quad \text{in } U_1.$$

Choose any open subset $V \subset\subset U_1$ with C^2-boundary such that $\{\mathbf{r}_1,\dots,\mathbf{r}_{N_m}\} \subset V$. Then interior H^2-estimate, cf. [38, Section 6.3.1], implies that

$$\|u_{\mathrm{R},n}\|_{H^2(V)} \le M_6$$

for some constant $M_6 > 0$ independent of n. By the Rellich-Kondrachov embedding theorem, cf. [39, Theorem 6.3], we have $H^2(V) \overset{c}{\hookrightarrow} W^{1,5}(V) \hookrightarrow C(V)$.

Together with (2.36), this implies that $u_{\mathrm{R},n}$ converge to $u_{\mathrm{R},\Gamma}$ pointwise in V. We thus conclude that

$$\begin{aligned}\lim_{n\to\infty} \int_\Omega \sum_{j=1}^{N_m} q_j \delta(\mathbf{r}-\mathbf{r}_j) u_{\mathrm{R},n}(\mathbf{r})\, d\mathbf{r} &= \lim_{n\to\infty} \sum_{j=1}^{N_m} q_j u_{\mathrm{R},n}(\mathbf{r}_j) \\ &= \sum_{j=1}^{N_m} q_j u_{\mathrm{R},\Gamma}(\mathbf{r}_j) \\ &= \int_\Omega \sum_{j=1}^{N_m} q_j \delta(\mathbf{r}-\mathbf{r}_j) u_{\mathrm{R},\Gamma}(\mathbf{r})\, d\mathbf{r}.\end{aligned}$$

Due to the expressions (2.43) and (2.44), this completes the proof. □

Remark 2.8. We will state several extensions of the results in Sections 2.2 and 2.3 in this remark.

(1) The reason to assume that $\{S_n\}_{n=1}^\infty$ satisfy (S2) and are C^2-continuous is to keep the definition of smeared surface functions consistent with those in [22]. A careful examination of the proofs of Proposition 2.3, Theorems 2.6 and 2.7 reveals that they do not rely on these two conditions. Therefore, assuming that $\{S_n\}_{n=1}^\infty : \Omega \to [0,1]$ is a sequences of $L^\infty-$functions satisfying Properties (S0) and (S1), the assertions in Proposition 2.3, Theorems 2.6 and 2.7 remain valid.

(2) Proposition 2.3, Theorems 2.6 and 2.7 are still true when Ω is a general bounded Lipschitz domain. This can be observed from the following way of decomposing $\widetilde{u}_d = \widetilde{u}_{L,d} + \widetilde{u}_{N,d}$ such that $\widetilde{u}_{L,d}$ solves

$$\begin{cases} -\nabla\cdot(\epsilon_d \nabla u) &= \nabla\cdot(\hat{\epsilon}_d \nabla u_C) \quad \text{in} \quad \Omega; \\ u &= u_b - u_C \quad \text{on} \quad \partial\Omega, \end{cases} \tag{2.45}$$

and $\widetilde{u}_{N,d}$ solves

$$\begin{cases} -\nabla\cdot(\epsilon_d \nabla u) + (1-S)\kappa^2 \sinh(u + u_C + \widetilde{u}_{L,d}) &= 0 \quad \text{in} \quad \Omega; \\ u &= 0 \quad \text{on} \quad \partial\Omega. \end{cases}$$

[36, Theorems 8.3 and 8.16] imply that $\widetilde{u}_{L,d} \in H^1(\Omega)$ with $\|\widetilde{u}_{L,d}\|_{L^\infty(\Omega)} \le M_7$ for some constant M_7 independent of S. Pick $w \in H^1(\Omega)$ with trace $u_b - u_C$ on $\partial\Omega$. Then multiplying both sides of (2.45) by $\widetilde{u}_{L,d} - w$ and integrating over Ω yield

$$\int_\Omega \left[\epsilon_d \nabla \widetilde{u}_{L,d} \nabla(\widetilde{u}_{L,d} - w) + \hat{\epsilon}_d \nabla u_C \nabla(\widetilde{u}_{L,d} - w)\right] d\mathbf{r} = 0.$$

Then we can apply Hölder and Young's inequalities to obtain that

$$-\int_\Omega \epsilon_d \nabla \widetilde{u}_{L,d} \nabla w \, d\mathbf{r} \geq -\delta \|\nabla \widetilde{u}_{L,d}\|^2_{L^2(\Omega)} - L_1(\delta)\|\nabla w\|^2_{L^2(\Omega)}$$

and similarly

$$\left|\int_\Omega \hat{\epsilon}_d \nabla u_C \nabla \widetilde{u}_{L,d} \, d\mathbf{r}\right| \leq \delta \|\nabla \widetilde{u}_{L,d}\|^2_{L^2(\Omega)} + L_2(\delta)\|\nabla u_C\|^2_{L^2(\Omega\setminus U_1)},$$

for any $\delta > 0$ and a continuous and decreasing functions $L_i : \mathbb{R}_+ \to \mathbb{R}_+$. Choosing δ sufficiently small, we infer that

$$\|\nabla \widetilde{u}_{L,d}\|_{L^2(\Omega)} \leq M_8$$

for some $M_8 > 0$ independent of S. On the other hand, by the Poincaré inequality

$$\begin{aligned}\|\widetilde{u}_{L,d}\|_{L^2(\Omega)} \leq & \|\widetilde{u}_{L,d} - w\|_{L^2(\Omega)} + \|w\|_{L^2(\Omega)} \leq C\|\nabla(\widetilde{u}_{L,d} - w)\|_{L^2(\Omega)} + \|w\|_{L^2(\Omega)} \\ \leq & C\|\nabla \widetilde{u}_{L,d}\|_{L^2(\Omega)} + C\|\nabla w\|_{L^2(\Omega)} + \|w\|_{L^2(\Omega)} \leq M_9\end{aligned}$$

for some $M_9 > 0$ independent of S. Then following the proof of Theorem 2.6, one can show that

$$\|\widetilde{u}_{N,d}\|_{H^1(\Omega)} + \|\widetilde{u}_{N,d}\|_{L^\infty(\Omega)} \leq M_{10}$$

for some $M_{10} > 0$ independent of S. Combining the above discussions, we thus obtain a uniform estimate for $\widetilde{u}_d$, which is independent of S. Then the assertions in Proposition 2.3, Theorems 2.6 and 2.7 follow by similar arguments to their original proofs.

(3) The energy convergence actually holds for more general forms of electrostatic solvation energy that include the entropic contributions from the ionic concentrations, e.g. [40, Equation (5.5)]. Based on (2.23) and (2.37), the convergence of the entropic terms can be established by using the dominated convergence theorem.

3. Numerical experiments

In this section, we will numerically investigate the convergence of the diffuse interface PB model to the sharp interface one. In all studies, the dielectric coefficients are chosen as $\epsilon_m = 1$ and $\epsilon_s = 80$, and the ionic strength is taken as $I = 0.15$ M. A uniform mesh with the spacing h being the same in x, y, and z directions is used. The unit of all lengths is Å.

We first consider a diatomic system with both radii being $R = 2$. Two test sets are studied with centers being $(\pm 2, 0, 0)$ and $(\pm 3, 0, 0)$, respectively, for Set 1 and Set 2. In our computations, we take a fixed domain $[-9, 9] \times [-6, 6] \times [-6, 6]$ and $h = 0.1$ for both sets. Following [22], the diffuse interfaces in both sets are constructed by using the Gaussian convolution surface (GCS), in which the limiting sharp interface Γ is defined as the solvent accessible surface (SAS) [5] with the probe radius being 1.5. Define the molecule domain Ω_m to be the region enclosed by the SAS. Consider a sequence of σ_n values of the Gaussian kernel approaching zero. For each σ_n value, the diffuse interface is generated by convoluting χ_{Ω_m} with the Gaussian kernel. After post-processing [22], this generates the smeared surface function $S_n(\mathbf{r})$. The GCS diffuse interfaces for Set 1 and Set 2 are illustrated, respectively, in Figs. 1 and 2. It is clear in both sets that as σ_n goes to zero, the GCS diffuse interface approaches to the corresponding SAS. We note that the SAS involves two cusps for the diatomic system. By pulling two balls away from each other, the cusps of the Set 2 is more evident. On the other hand, we can see that the GCS surfaces are all very smooth, including at corner points. Because of smooth dielectric profile, a simple finite difference algorithm is sufficient for solving the diffuse interface PB equation [22].

By considering a diffuse interface with a given σ_n^2 value, the corresponding electrostatic free energy E_n of the diatomic system is numerically calculated by solving the linearized PB equation with the regularization method developed in [22]. The calculated energies are listed in Table 1. It can be seen that as σ_n^2 becomes smaller, E_n becomes larger. Moreover, the energies of two sets are plotted against σ_n^2 in part (a) and (b) of Fig. 3. A convergence pattern is clearly seen for both sets.

For a comparison, the regularized Matched Interface and Boundary (rMIB) method [8] is employed to solve the linearized PB equation for both diatomic systems. Numerically, the rMIB method utilizes a sophisticated finite difference algorithm for treating the complex geometry of the molecular surface and for enforcing interface jump conditions so that a second order of accuracy can be guaranteed. Moreover, as mentioned above, the regularization utilized in the rMIB method is essentially equivalent to the regularized PB Eq. (2.5).

However, the existing rMIB package cannot handle the SAS directly. Instead, the rMIB method is designed for the solvent excluded surface (SES) which is known to be smoother than the SAS [6]. In the present study, to mimic the sharp interface limit of the GCS, we first augment the atom radii by adding 1.5Å for each ball. Then a SES is generated based on the augmented diatomic structure by using the software MSMS [41] with a probe radius being 1.5Å. The resulting molecular surface will be called rMIB sharp interface in this paper. The rMIB sharp interfaces of Set 1 and Set 2 are shown, respectively, in Figs. 1 and 2. It is seen that the rMIB sharp interface is identical to the SAS for most regions. However, at the overlapping region between two balls, the rMIB molecular surface becomes fatter, and is free of the cusps. Physically, because the solute domain enclosed by the rMIB sharp interface is larger than that of the SAS, the rMIB energy is larger than the limiting energy of the GCS method. Consequently, the rMIB energies for both sets are well above those of the GCS, as can be seen in both Table 1 and Fig. 3.

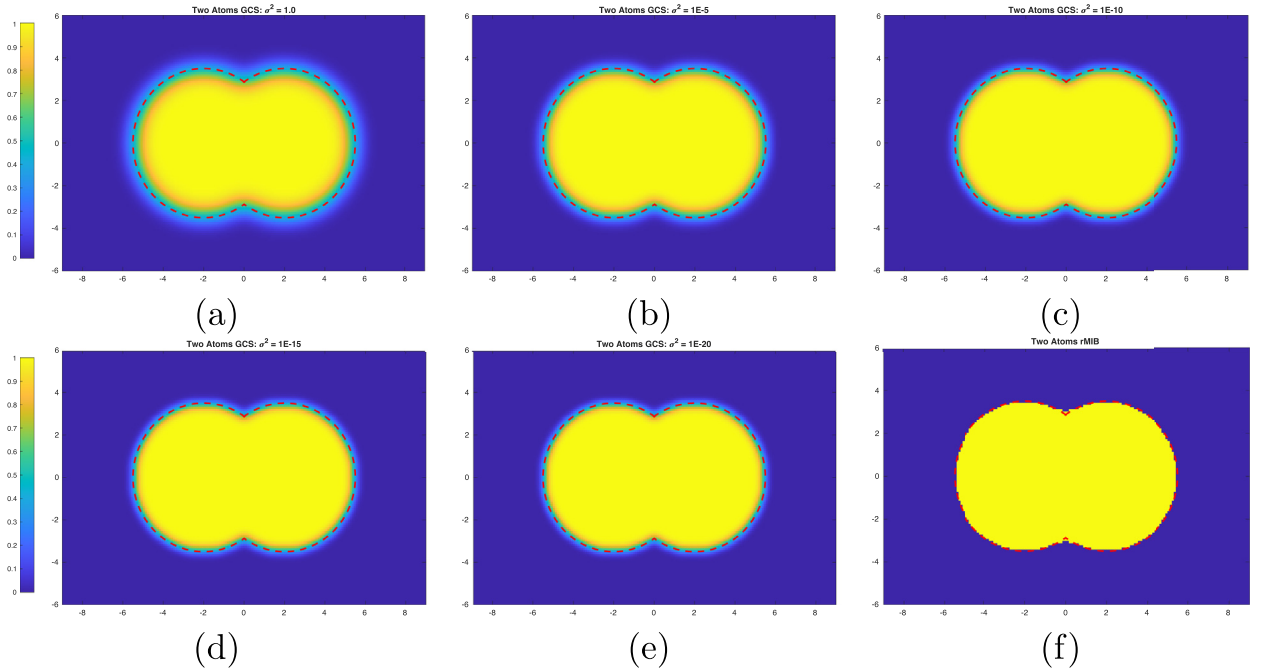

Fig. 1. Heat-map plots for the diatomic system Set 1. In (a) - (e), the GCS diffuse interface is generated by setting $\sigma^2 = 1$, 1×10^{-5}, 1×10^{-10}, 1×10^{-15}, and 1×10^{-20}, respectively. In (f), the rMIB sharp interface is shown. In all figures, the SAS is shown as dash lines.

Table 1
Electrostatic free energies (kcal/mol) calculated by using the GCS diffuse interface with different σ_n^2 values. For a comparison, the energies calculated by the rMIB method with a sharp interface are also given.

Method	σ_n^2	E_n			
		Set 1	Set 2	1AHO	1CBN
GCS	1	-210.3648	-191.8235	-630.5557	-243.2320
	5×10^{-1}	-208.3573	-190.0311	-611.1638	-233.5578
	1×10^{-1}	-204.2312	-186.2760	-575.5727	-215.9419
	1×10^{-3}	-195.7454	-178.7213	-516.5366	-187.2860
	1×10^{-5}	-190.4240	-174.0887	-485.0368	-172.6137
	1×10^{-10}	-183.1100	-167.8359	-437.8402	-151.6080
	1×10^{-15}	-179.2319	-164.5767	-410.6039	-139.2410
	1×10^{-20}	-176.7700	-162.5300	-400.4246	-133.3438
rMIB	–	-156.4009	-145.0452	-228.3870	-71.7445

Next, we consider the convergence of electrostatic free energy for two real proteins with protein databank (PDB) ID: 1AHO and 1CBN. The protein structures are prepared as explained in [19]. The rMIB sharp interfaces of two proteins are shown in Fig. 4, which are the SES generated based on enlarged atoms. For a comparison, the GCS surfaces of two proteins are illustrated at $S(x, y, z) = 0.5$ for $\sigma_n^2 = 1$. The GCS isosurfaces are obviously very smooth with $\sigma_n^2 = 1$, while the rMIB sharp interfaces contain many atomic features. In protein computations, we take $h = 0.5$ Å, and a large enough cubic domain Ω is employed for each protein. The GCS and rMIB energies are also reported in Table 1 and Fig. 3. Again, the GCS energy is approaching certain limit as σ_n^2 goes to zero, which shall be smaller than the corresponding rMIB energy, because the rMIB sharp interface is always larger than the SAS.

The present studies indicate that the energy convergence of the GCS diffuse interface cannot be precisely verified in numerical computations. This is limited by two numerical factors. First, due to the limitation of numerical algorithms, one cannot use the SAS in the rMIB algorithm. Instead, an enlarged sharp interface has to be used, which produces a large energy value as the reference for the sharp interface case. The second limiting factor is the numerical resolution. When σ_n is very small, $\nabla\epsilon$ undergoes a rapid while smooth change at the solute-solvent boundary. Unless an extremely small mesh spacing h is used, the finite difference method is unstable to capture such change. However, such a computation involves an extremely dense mesh, and becomes prohibitively expensive. In summary, it is concluded that the convergence of the GCS energy towards its sharp interface limit is impossible to be realized numerically. This is essentially why a theoretical proof is needed, which is the motivation of this study.

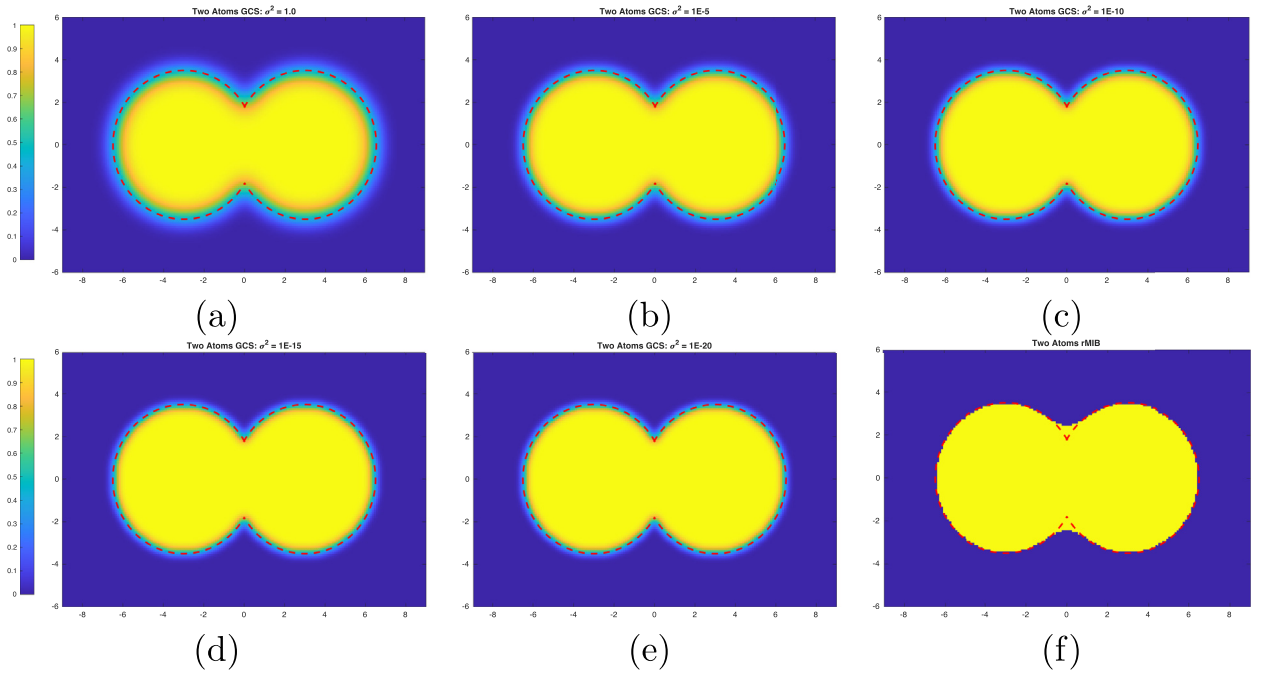

Fig. 2. Heat-map plots for the diatomic system Set 2. In (a) - (e), the GCS diffuse interface is generated by setting $\sigma^2 = 1$, 1×10^{-5}, 1×10^{-10}, 1×10^{-15}, and 1×10^{-20}, respectively. In (f), the rMIB sharp interface is shown. In all figures, the SAS is shown as dash lines.

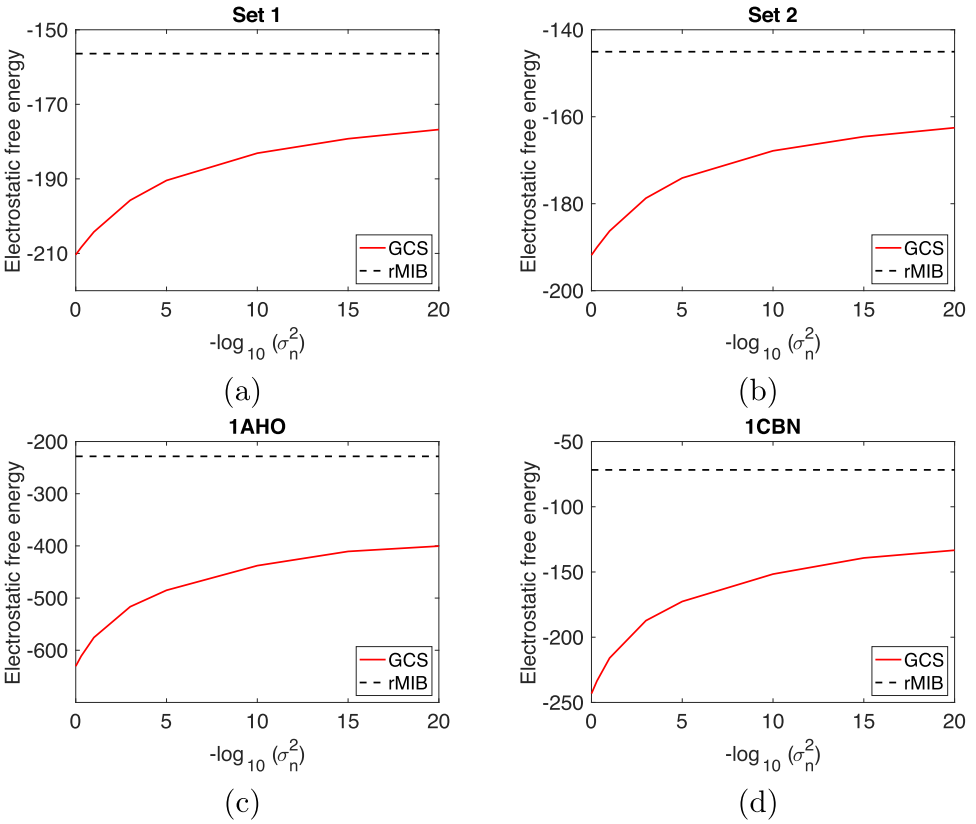

Fig. 3. As σ goes to zero, the electrostatic free energy E_n calculated by the GCS regularization method is approaching certain limit. For a comparison, the energy calculated by the rMIB algorithm for a sharp interface is also plotted. (a). Diatomic system Set 1; (b). Diatomic system Set 2; (c). 1AHO; (d). 1CBN.

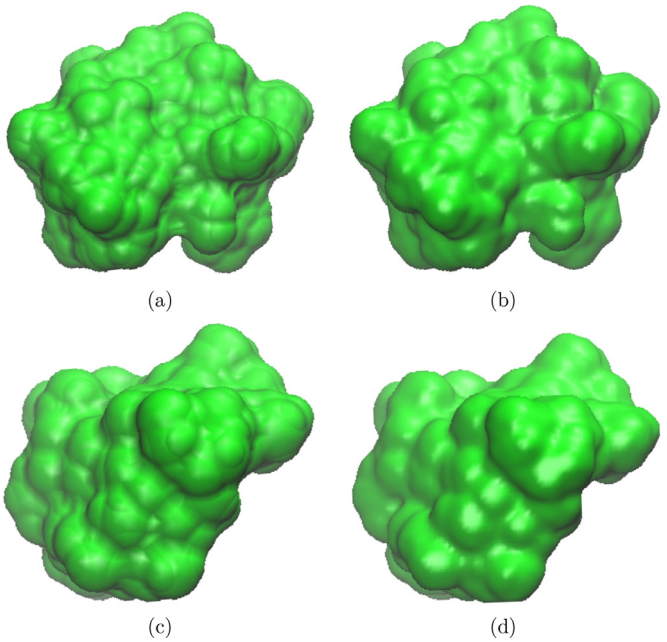

Fig. 4. Molecular surfaces of two proteins. In (a) and (c), the rMIB sharp interface is plotted for 1AHO and 1CBN, respectively. In (b) and (d), an isosurface $S(x, y, z) = 0.5$ is plotted for the GCS surfaces of 1AHO and 1CBN, respectively, which are generated by using $\sigma_n^2 = 1$.

4. Conclusion

The significance of the work is twofold. First, we investigated the convergence of a diffuse interface PB model to the sharp interface PB model, both numerically and theoretically. Due to the limitation in numerical algorithm and mesh resolution, we found that the convergence of electrostatic free energy is impossible to be realized numerically. Instead, we rigorously proved the convergence for both the regularized potential and electrostatic free energy.

Second, the regularizations for both diffuse interface and sharp interface PB models are unified into one framework. For the diffuse interface model, we adopted the two-component regularization of [22] to decompose the potential into a reaction-field component and a Coulomb component, with the latter being calculated analytically by Green's functions to account for singular charges. The reaction-field component then satisfies a regularized PB equation with a smooth source. The regularization for the sharp interface PB equation is formulated in the same manner, in which the source term is the sharp interface limit of the one for the diffuse interface model. The connection between the present sharp interface PB regularization and the existing two-component scheme [23,27] has been discussed. In particular, the preserved source term for accuracy recovery in [34] is essentially equivalent to the present formulation.

In summary, the unified regularization of this work will provide a theoretical foundation for treating charge singularities for more complicated PB models, such as various diffuse interface PB models [10–17] and the concentration dependent dielectric PB model [42]. For the modified PB model [42], the numerical discretization of the new source term $\nabla \cdot (\hat{\epsilon}_d \nabla u_C)$ demands further studies in dealing with a heterogeneous dielectric function in the solvent region and a dielectric jump at the solute-solvent boundary. On the other hand, the present regularization has been further advanced in treating partial charges in the super-Gaussian PB model, in which the dielectric function is heterogeneous in the solute region, but is required to be almost flat in a small neighborhood surrounding each atom center [43].

Data Availability

Data sharing is not applicable to this article as no datasets were generated or analyzed during the study.

Acknowledgments

Zhao's research was partially supported by the National Science Foundation (NSF) under grant DMS-1812930 and DMS-2110914. Alexov's research was partially supported by the National Institutes of Health (NIH) under grants R01GM093937, R01GM125639 and P20GM121342.

References

[1] K.A. Sharp, B. Honig, Electrostatic interactions in macromolecules - theory and applications, Annu. Rev. Biophys. Biophys. Chem. 19 (1990) 301–332.
[2] B. Honig, A. Nicholls, Classical electrostatics in biology and chemistry, Science 268 (5214) (1995) 1144–1149.
[3] N.A. Baker, Improving implicit solvent simulations: a Poisson-centric view, Curr. Opin. Struct. Biol. 15 (2) (2005) 137–143, doi:10.1016/j.sbi.2005.02.001.
[4] M.J. Holst, The Poisson-Boltzmann equation: analysis and multilevel numerical solution, UIUC, 1994 Ph.D. thesis.
[5] B. Lee, F.M. Richards, The interpretation of protein structures: estimation of static accessibility, J. Mol. Biol. 55 (3) (1971) 379–IN4.
[6] F.M. Richards, Areas, volumes, packing, and protein structure, Annu. Rev. Biophys. Bioeng. 6 (1) (1977) 151–176.
[7] J.A. Grant, B. Pickup, A Gaussian description of molecular shape, J. Phys. Chem. 99 (11) (1995) 3503–3510.
[8] W. Geng, S. Zhao, A two-component matched interface and boundary (MIB) regularization for charge singularity in implicit solvation, J. Comput. Phys. 351 (2017) 25–39.
[9] S. Ahmed Ullah, S. Zhao, Pseudo-transient ghost fluid methods for the Poisson-Boltzmann equation with a two-component regularization, Appl. Math. Comput. 380 (2020) 125267, doi:10.1016/j.amc.2020.125267. http://www.sciencedirect.com/science/article/pii/S0096300320302368.
[10] A. Abrashkin, D. Andelman, H. Orland, Dipolar Poisson-Boltzmann equation: ions and dipoles close to charge interfaces, Phys. Rev. Lett. 99 (7) (2007) 077801.
[11] P.W. Bates, G.-W. Wei, S. Zhao, Minimal molecular surfaces and their applications, J. Comput. Chem. 29 (3) (2008) 380–391.
[12] P. Bates, Z. Chen, Y. Sun, G.-W. Wei, S. Zhao, Geometric and potential driving formation and evolution of biomolecular surfaces, J. Math. Biol. 59 (2) (2009) 193–231.
[13] L.-T. Cheng, J. Dzubiella, J.A. McCammon, B. Li, Application of the level-set method to the implicit solvation of nonpolar molecules, J. Chem. Phys. 127 (8) (2007) 084503.
[14] Y. Zhao, Y.-Y. Kwan, J. Che, B. Li, J.A. McCammon, Phase-field approach to implicit solvation of biomolecules with coulomb-field approximation, J. Chem. Phys. 139 (2) (2013) 024111.
[15] S. Dai, B. Li, J. Lu, Convergence of phase-field free energy and boundary force for molecular solvation, Arch. Ration. Mech. Anal. 227 (1) (2018) 105–147, doi:10.1007/s00205-017-1158-4.
[16] Y. Shao, E. Hawkins, K. Wang, Z. Chen, A constrained variational model of biomolecular solvation and its numerical implementation, Comput. Math. Appl. 107 (2022) 17–28, doi:10.1016/j.camwa.2021.12.009.
[17] Z. Chen, Y. Shao, A new approach to constrained total variation solvation models and the study of solute-solvent interface profiles, arXiv preprint arXiv:2203.11285.
[18] L. Li, C. Li, Z. Zhang, E. Alexov, On the dielectric “Constant” of proteins: smooth dielectric function for macromolecular modeling and its implementation in Delphi, J. Chem. Theory Comput. 9 (4) (2013) 2126–2136.
[19] A. Chakravorty, Z. Jia, L. Li, S. Zhao, E. Alexov, Reproducing the ensemble average polar solvation energy of a protein from a single structure: gaussian-based smooth dielectric function for macromolecular modeling, J. Chem. Theory Comput. 14 (2) (2018) 1020–1032.
[20] T. Hazra, S.A. Ullah, S. Wang, E. Alexov, S. Zhao, A super-Gaussian Poisson–Boltzmann model for electrostatic free energy calculation: smooth dielectric distribution for protein cavities and in both water and vacuum states, J. Math. Biol. 79 (2) (2019) 631–672.
[21] S.K. Panday, M.H. Shashikala, A. Chakravorty, S. Zhao, E. Alexov, Reproducing ensemble averaged electrostatics with super-Gaussian-based smooth dielectric function: application to electrostatic component of binding energy of protein complexes, Commun. Inf. Syst. 19 (4) (2019).
[22] S. Wang, E. Alexov, S. Zhao, On regularization of charge singularities in solving the poisson-Boltzmann equation with a smooth solute-solvent boundary, Math. Biosci. Eng. 18 (2) (2021) 1370–1405.
[23] L. Chen, M.J. Holst, J. Xu, The finite element approximation of the nonlinear Poisson–Boltzmann equation, SIAM J Numer Anal 45 (6) (2007) 2298–2320.
[24] D. Xie, New solution decomposition and minimization schemes for Poisson-Boltzmann equation in calculation of biomolecular electrostatics, J. Comput. Phys. 275 (2014) 294–309, doi:10.1016/j.jcp.2014.07.012.
[25] A. Nicholls, B. Honig, A rapid finite difference algorithm, utilizing successive over-relaxation to solve the Poisson–Boltzmann equation, J. Comput. Chem. 12 (4) (1991) 435–445.
[26] W. Deng, J. Xu, S. Zhao, On developing stable finite element methods for pseudo-time simulation of biomolecular electrostatics, J. Comput. Appl. Math. 330 (2018) 456–474.
[27] Z. Zhou, P. Payne, M. Vasquez, N. Kuhn, M. Levitt, Finite-difference solution of the Poisson–Boltzmann equation: complete elimination of self-energy, J. Comput. Chem. 17 (11) (1996) 1344–1351.
[28] I.-L. Chern, J.-G. Liu, W.-C. Wang, et al., Accurate evaluation of electrostatics for macromolecules in solution, Methods Appl. Anal. 10 (2) (2003) 309–328.
[29] W. Geng, S. Yu, G. Wei, Treatment of charge singularities in implicit solvent models, J. Chem. Phys. 127 (11) (2007) 114106.
[30] Q. Cai, J. Wang, H.-K. Zhao, R. Luo, On removal of charge singularity in Poisson–Boltzmann equation, J. Chem. Phys. 130 (14) (2009) 04B608.
[31] M. Holst, J.A. McCammon, Z. Yu, Y.C. Zhou, Y. Zhu, Adaptive finite element modeling techniques for the Poisson-Boltzmann equation, Commun. Comput. Phys. 11 (1) (2012) 179–214, doi:10.4208/cicp.081009.130611a.
[32] P. Benner, V. Khoromskaia, B. Khoromskij, C. Kweyu, M. Stein, Computing electrostatic potentials using regularization based on the range-separated tensor format, arXiv preprint arXiv:1901.09864(2019).
[33] B.N. Khoromskij, Range-separated tensor decomposition of the discretized Dirac delta and elliptic operator inverse, J. Comput. Phys. 401 (2020) 108998, doi:10.1016/j.jcp.2019.108998.
[34] A. Lee, W. Geng, S. Zhao, Regularization methods for the Poisson-Boltzmann equation: comparison and accuracy recovery, J. Comput. Phys. 426 (2021) 109958, doi:10.1016/j.jcp.2020.109958. https://www.sciencedirect.com/science/article/pii/S0021999120307324.
[35] S. Wang, A. Lee, E. Alexov, S. Zhao, A regularization approach for solving Poisson’s equation with singular charge sources and diffuse interfaces, Appl. Math. Lett. 102 (2020) 106144, doi:10.1016/j.aml.2019.106144. https://www.sciencedirect.com/science/article/pii/S0893965919304689.
[36] D. Gilbarg, N.S. Trudinger, Elliptic partial differential equations of second order, Grundlehren der Mathematischen Wissenschaften [Fundamental Principles of Mathematical Sciences], vol. 224, second ed., Springer-Verlag, Berlin, 1983, doi:10.1007/978-3-642-61798-0.
[37] S.J. Fromm, Potential space estimates for Green potentials in convex domains, Proc. Amer. Math. Soc. 119 (1) (1993) 225–233, doi:10.2307/2159846.
[38] L.C. Evans, Partial differential equations, Graduate Studies in Mathematics, vol. 19, second ed., American Mathematical Society, Providence, RI, 2010, doi:10.1090/gsm/019.
[39] R.A. Adams, J.J.F. Fournier, Sobolev spaces, Pure and Applied Mathematics (Amsterdam), vol. 140, second ed., Elsevier/Academic Press, Amsterdam, 2003.
[40] B. Li, Minimization of electrostatic free energy and the Poisson-Boltzmann equation for molecular solvation with implicit solvent, SIAM J. Math. Anal. 40 (6) (2009) 2536–2566, doi:10.1137/080712350.
[41] M.F. Sanner, A.J. Olson, J.-C. Spehner, Reduced surface: an efficient way to compute molecular surfaces, Biopolymers 38 (3) (1996) 305–320, doi:10.1002/(SICI)1097-0282(199603)38:3<305::AID-BIP4>3.0.CO;2-Y.
[42] X. Ji, S. Zhou, Variational approach to concentration dependent dielectrics with the Bruggeman model: theory and numerics, Commun. Math. Sci. 17 (7) (2019) 1949–1974.
[43] S. Wang, Y. Shao, E. Alexov, S. Zhao, A regularization approach for solving the super-Gaussian Poisson-Boltzmann model with heterogeneous dielectric functions, J. Comput. Phys. 464 (2022) 111340, doi:10.1016/j.jcp.2022.111340. https://www.sciencedirect.com/science/article/pii/S0021999122004028.